

Resonant scattering of matter wave gap-solitons by optical lattice defects

Valeriy A. Brazhnyi¹ and Mario Salerno²

¹*Centro de Física do Porto, Faculdade de Ciências,*

Universidade do Porto, R. Campo Alegre 687, Porto 4169-007, Portugal

²*Dipartimento di Fisica "E. R. Caianiello", CNISM and INFM Gruppo Collegato di Salerno,*

Università di Salerno, via Ponte don Melillo I-84084, Fisciano (SA), Italy

(Dated: February 5, 2022)

The physical mechanism underlying scattering properties of matter wave gap-solitons by linear optical lattice defects is investigated. The occurrence of repeated reflection, transmission and trapping regions for increasing strengths of an optical lattice defect are shown to be due to impurity modes inside the defect potential with chemical potentials and numbers of atoms matching corresponding quantities of an incoming gap-soliton. For gap-solitons with chemical potentials very close to band edges, the number of resonances observed in the scattering coincides with the number of bound states which can exist in the defect potential for the given defect strength. The dependence of the positions and widths of the transmission resonant on the incoming gap-soliton velocities are investigated by means of a defect mode analysis and effective mass theory. The comparisons with direct integrations of the Gross-Pitaevskii equation provide a very good agreement confirming the correctness of our interpretation. The possibility of multiple resonant transmission through arrays of optical lattice defects is also demonstrated. In particular, we show that it is possible to design the strength of the defects so to balance the velocity detunings and to allow the resonant transmission through a larger number of defects. The possibility of using these results for very precise gap-soliton dynamical filters is suggested.

PACS numbers: 03.75.Lm, 03.75.Kk, 03.75.-b

I. INTRODUCTION

Bose-Einstein condensates (BECs) in optical lattices (OLs) are presently attracting a great deal of interest [1] due both to their flexibility in parameter design and to the possibility they offer to observe interesting phenomena such as superfluid to Mott-insulator transition [2], Bloch oscillations [3], Landau-Zener tunneling [4, 5], generation of coherent atomic pulses (atom laser) [6], atom interferometry [7], etc. In this respect, OLs allow to control important properties of BEC by means of their periodic structure, this allowing, for example, the existence and stability of localized nonlinear excitations with chemical potentials inside band-gaps (so called gap-solitons (GSs)) even in the presence of repulsive interactions (positive scattering lengths). This fact, that would be obviously impossible in absence of the OL [8], has been experimentally demonstrated in [9].

Modulations of the OL can be used to accelerate, decelerate or to scatter GSs as well as to control their velocities [10]. Uniform accelerations of the OL combined with periodic modulations of the scattering length, either in space or in time, were shown to be effective tools to induce long-lived Bloch oscillations in the nonlinear regime [11], as well as band-gap tunneling phenomena such as the Landau-Zener tunneling [12]. Periodic time dependent OL accelerations were also used to achieve the dynamical localization of nonlinear matter waves [13, 14] and the Rabi-oscillations of GS states across a band-gaps [15] which survive on a long time scale in the presence of nonlinearity. Moreover, the combination of the above phenomena permits the stirring of GSs both in the reciprocal and in the direct lattice space as recently

demonstrated in [16]. Besides the one-dimensional contexts in which these effects have been investigated, OLs also play an important role for stabilizing GSs against collapse or decay in higher dimensions [17].

All what said above refers to the case of perfect OLs, e.g. OLs without distortions or defects which compromise the periodicity structure. In this case the interplay between periodicity and nonlinearity is the only source for the localization of matter waves in the system. OL defects, however, introduce additional bound states in the band-gaps (so called impurity modes) [18] providing an alternate source of localization in the system. Opposite to GSs, impurity modes exist both in absence and in presence of nonlinearity and can interfere in the scattering process of GSs by OL defects.

Scattering properties of solitons with single (non periodic) potential wells have been extensively investigated during the past years. For the case of the nonlinear Schrödinger equation (NLSE) scattering of solitons by extended defects were numerically investigated in [19] where the occurrence of a series of reflection, transmission, and trapping regions as a function of the defect strength was reported. A similar problem has been recently investigated for solitons of the Gross-Pitaevskii equation (GPE) with rectangular potential wells and for attractive interatomic interactions [20].

Similar studies were also done for point defects of the discrete NLSE equation [21–24] which corresponds, under suitable conditions, to a tight-binding model of BEC in a deep OL [25]. The resonant transmission, reflection and trapping of discrete breathers by point-defects was investigated in [26]. In contrast to these studies, however, the scattering of continuous GPE GSs by OL defects have

been scarcely investigated. In this context, we mention the numerical study performed in [27] where the scattering properties of GSs were suggested to be useful to construct quantum switches and quantum memories. To our knowledge, however, the mechanism underlying resonant transmissions of GPE GSs by OL defects and the possibility of multiple defects resonant scattering have not yet been discussed.

In the present paper we provide an extensive numerical investigation of the scattering properties of GSs by OL defects and identify the physical mechanism underlying the phenomenon of the resonant transmission. In particular, we show that the presence of repeated reflections transmission and trapping regions observed for increasing strengths of an OL defect is associated to the impurity modes inside the defect potential with energies (chemical potentials) and numbers of atoms matching corresponding quantities of the incoming GS. As the OL defect strength is increased, new impurity modes enter from the gap edges, moving toward the center of the gap (bottom of the potential). This implies that for incoming GSs with chemical potentials very close to band edges, the number of resonances observed in the scattering coincides with the number of bound states which can exist in the defect potential for the given defect strength. This fact is demonstrated both by studying stationary states inside the defect potential and by direct numerical integrations of the GPE. An excellent agreement between the two approaches is found, this confirming the correctness of our interpretation.

The dependence of the resonant transmission on the incoming velocity of the GS is also investigated both for fundamental GSs in the semi-infinite gap and for GSs in the first gap zone. As a result we show that the transmission resonant peaks become wider as the incoming velocity is increased, with very sharp peaks at small velocities. The multiple resonant transmission through a series of (two and three) OL defects is also demonstrated. We show in this case that for equally spaced identical OL defects the widths of the full transmission resonances in general decreases as the number of defects is increased. We demonstrate, however, that the resonant transmission through a series of defects can be achieved if defects are designed so to compensate off-resonance detunings introduced by velocity changes. This fact gives rise to the possibility of using arrays of OL defects as very precise filters for matter wave dynamics.

The paper is organized as follows. In Sec. II we present the model equation and discuss the basic properties of GSs of the GPE. In the Sec. III we consider the interaction of small amplitude GSs with a localized Gaussian impurity in the OL. The problem is investigated by means of direct numerical integrations of the GPE for both attractive and repulsive interactions as well as for attractive and repulsive defects. In section IV we use a stationary defect mode analysis to show that the repeated resonant transmission, reflection and trapping regions occurs in correspondence of resonances with impurity modes inside

the defect potential and investigate their dependence on GS incoming velocities. In section V the multiple resonant transmission across a series of equidistant (equal and unequal) OL defects, is investigated. In Sect. VI the main results of the paper are shortly resumed.

II. MODEL EQUATION AND STATIONARY LOCALIZED SOLUTIONS

Let us consider a cigar-shaped BEC described by the following normalized one-dimensional GPE [1, 28]

$$i\frac{\partial\psi}{\partial t} = -\psi_{xx} + V_{ext}(x)\psi + \sigma|\psi|^2\psi, \quad (1)$$

where $V_{ext}(x)$ denotes an external potential of the form: $V_{ext}(x) = V_{ol}(x) + V_d(x)$, with $V_{ol}(x)$ a perfect OL of period L : $V_{ol}(x) = V_{ol}(x+L)$, and $V_d(x)$ a defect potential consisting of a sum of n_d single wells potentials localized on a distance of several lattice period around the OL sites x_i , $i = 1, \dots, n_d$. In the following we assume V_{ol} and V_d to have the form

$$V_{ol}(x) = V_0 \cos(2x), \quad (2)$$

$$V_d(x) = \sum_{i=1}^{n_d} \frac{\eta_i}{\sqrt{2\pi}\Delta_i} \exp[-(x-x_i)^2/(2\Delta_i^2)] \quad (3)$$

where without loss of generality the period of the OL is taken π . We remark that results of this paper will not qualitatively dependent on type of defect (we used Gaussian defects just for numerical convenience) and similar results can be obtained for other shapes of the defects, like square well defects, for example). In the following we will mainly restrict to the cases of few OL defects: $n_d = 1, 2, 3$, only. We also remark that in Eq.(1) the normalization has been made by measuring the energy in units of recoil energy $E_r = \hbar^2 k^2 / (2m)$, where $k = \pi/d$ and d is the lattice constant, the space coordinate and time in units of d/π and E_r/\hbar , respectively. The dimensionless macroscopic wave function is also normalized as $\int |\psi|^2 dx = 8\pi Nk|a_s|$, where a_s is the s-wave scattering length.

It is well known that in the absence of the defect potential $V_d \equiv 0$, Eq.(1) posses families of exact GS solutions with energy located in the band-gaps of the linear eigenvalue problem

$$\frac{d^2\varphi_{\alpha k}}{dx^2} + [E_{\alpha}(k) - V_{ol}(x)]\varphi_{\alpha k} = 0, \quad (4)$$

where $\varphi_{\alpha k}(x)$ are orthonormal set of Bloch functions with α denoting the band index and k the crystal-momentum inside the first Brillouin zone (BZ): $k \in [-1, 1]$. It is also known that small-amplitude GSs with chemical potentials E_s very close to band edges are of the form $\psi(x, t) = A(\zeta, \tau)\varphi_{\alpha k}(x)e^{-iE_{\alpha}(k)t}$ with the envelope function $A(\zeta, \tau)$ obeying the following NLSE

$$i\frac{\partial A}{\partial \tau} = -\frac{1}{2M_{eff}}\frac{\partial^2 A}{\partial \zeta^2} + \chi|A|^2 A \quad (5)$$

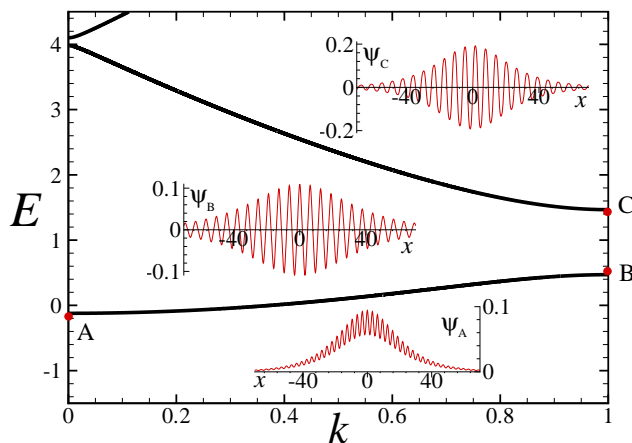


FIG. 1: Band-gap structure for $V_0 = -1$ and GS bound states at points A, B and C near band-gap edges, corresponding to chemical potentials $E_{A,B,C} = -0.125; 0.475; 1.452$, respectively. Insets show the wave functions $\psi_{A,B,C}$ of the bound states.

where τ and ζ are slow temporal and spatial variables, $M_{eff} = (d^2 E_\alpha / dk^2)^{-1}$ denotes the soliton effective mass and $\chi = \sigma \int |\varphi_{\alpha k}|^4 dx$ the effective nonlinearity [8]. The condition for the existence of such solitons is $\chi M_{eff} < 0$ and coincides with the condition for the modulational instability of the Bloch wavefunctions at the edges of the BZ [8]. Examples of small amplitude GSs with chemical potential inside the band-gap structure are depicted in Fig. 1.

In the presence of very diluted OL defects, GSs will continue to exist and away from defects they practically coincide with GSs of the undistorted OL. An attractive (local potential well) or repulsive (local potential barrier) OL defect will be seen by the GSs differently, depending on the sign of their effective mass. Thus, for example, in the case of repulsive interactions and a negative effective mass, a GS approaching a repulsive defect will see it as a trapping potential (rather than as a potential barrier), thus besides being totally or partially transmitted/reflected, it can also be trapped at the defect site, a fact which would be impossible in absence of the OL. In all the numerical simulations presented in this paper we have used stationary GSs of Eqs. (1)–(3), exactly determined by the shooting method [29] or by self-consistent calculations [30], and have put them in action by means of phase imprinting (e.g. we multiply the state by the phase factor $e^{-i\sigma v x/2}$, with v being the GS velocity). This provides initial condition for the GPE numerical time integration of the form: $\psi(x, 0) = \psi_s(x) e^{-i\sigma v x/2}$. For possible experimental implementations of our results, an alternate method to use to put the GS in action could be the acceleration of the OL for a short time interval to move the stationary state away from the BZ edges (center) so that it can acquire a small Bloch velocity $v_B = dE_\alpha(k)/dk \ll 1$ (for details on how this can be done see [16]).

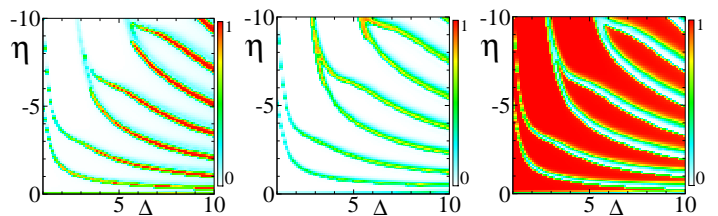


FIG. 2: Dependence of the transmission (left), trapping (center) and reflection (right) coefficients on the amplitude η and width Δ of the defect potential V_d . Parameters are $v = 0.05$, $E_s = -0.125$, $V_0 = -1$.

III. RESONANT SCATTERING OF GS BY AN OL DEFECT

We consider first the scattering of a GS by a single localized defect ($n_d = 1$ in Eq. (3)). In order not to perturb the soliton initially, the distance between the soliton center and the OL defect is taken much larger than the width of the GS ($\approx 80L$). In the following we compute the trapping, transmission and reflection coefficients defined as $C = N_C(t_f)/N_{ini}$, $T = N_T(t_f)/N_{ini}$ and $R = 1 - (T + C)$, with $N_C(t_f) = \int_{-x_c}^{x_c} |\psi(t_f)|^2 dx$, $N_T(t_f) = \int_{x_c}^{\infty} |\psi(t_f)|^2 dx$ and $N_{ini} = \int_{-\infty}^{\infty} |\psi(t=0)|^2 dx$ denoting the numbers of atoms trapped, transmitted and in the initial state, respectively. The final time t_f depends on the initial velocity of the GS and in the numerical experiment is determined as the time necessary for the coefficients T, R, C to become stationary after the scattering process has occurred. The trapping region $[-x_c, x_c]$ has the size of the initial soliton and in all our calculations we fix $x_c = 30L$.

A. Scattering of semi-infinite GS by an OL defect

For the scattering of a GS in the semi-infinite gap to occur, the existence criterion for a GS near the bottom edge of the first band (where the effective mass is positive) implies that the nonlinear coefficient must be negative sign(σ) = -1. By applying a small initial velocity to the GS in the defect direction, depending on the amplitude η and width Δ of the defect, three possible scenarios can occur: i) complete reflection, $R = 1$; ii) complete transmission, $T = 1$; iii) partial trapping, $C > 0$. The regions of the parameter space $\{\eta, \Delta\}$ where these different regimes occur, as obtained from direct numerical integration of Eq.(1), are reported in Fig. 2. The dependence of T, C, R on the defect strength η for two different incoming GS velocities and for a fixed value of the defect width $\Delta = 5$ is depicted in Fig. 3. We see that by changing the strength of the defect it is possible to achieve complete reflections ($R \approx 1$) or transmission ($T \approx 1$) as well as partial trappings ($C > 0$). The profiles of the initial, reflected and transmitted GS are depicted in the top panels of Fig.3 for defect strengths corresponding to points labeled in the middle panel by letters A, B, C. By

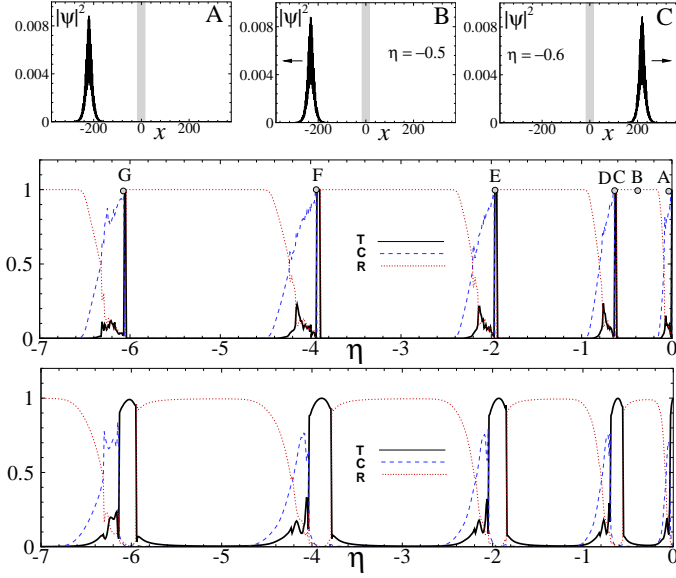


FIG. 3: Dependence of coefficients $T(\eta)$, $R(\eta)$ and $C(\eta)$ on the OL defect strength for two GS incoming velocities: $v = 0.01$ (middle panel) and $v = 0.05$ (bottom panel). The top panels A, B and C correspond to the profiles of initial, reflected and transmitted GS. The wide line in gray shows the position of the defect. Other parameters are $\Delta = 5$, $E_s = -0.125$, $V_0 = -1$.

comparing the middle and the bottom panels of Fig.3 it is clear that the sharp peaks at small incoming velocities ($v \approx 0$) for which $T \approx 1$ (see points A, C, E, F, G in the middle panel) become wider as the velocity is increased while the regions for which $R \approx 1$ are a bit reduced (also see Fig.5 for the case of first band-gap GSs).

The first four impurity modes corresponding to the transmission peaks D, E, F, G in the middle panel of Fig.3 have been depicted in Fig. 4. Notice the alternating odd-even symmetry of these modes (modes D and F being odd and modes E and G being even with respect to the center $x = 0$ of the defect potential) as usual for eigenstates of one-dimensional trapping potentials. We remark that the existence of four resonant transmission peaks (and reflection regions) seen in Fig.3 for $-7 \leq \eta < 0$ correlates with the existence of four impurity modes for the given defect strength region (see stationary defect mode analysis below).

B. Scattering of first band-gap GSs by an OL defect

Similar results as those of the previous section can be found for GSs inside the first band-gap, with the only difference that now there are two possibilities for the existence of small-amplitude solitons: i) in the vicinity of the top edge of the first band where the effective mass is negative and therefore GSs can exist only for repulsive interactions $\sigma = 1$; ii) and in the vicinity of the bottom

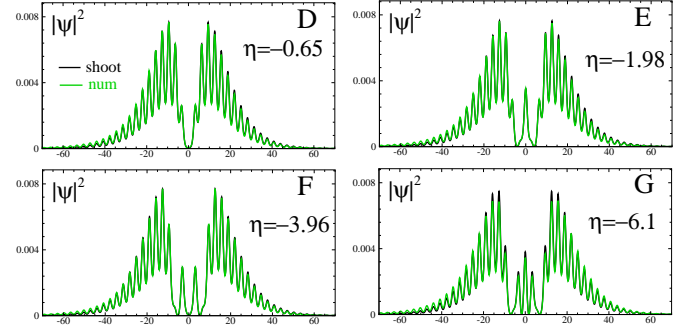


FIG. 4: Defect modes corresponding to the maxima of the trapping curves ($C \approx 1$) indicated in Fig.3 by letters D, E, F and G, respectively. Green lines correspond to the defect modes obtained from the dynamical GPE calculations while dark lines refer to defect mode profiles obtained from Eq.(8) (see below). Parameters are fixed as in Fig.3.

edge of the second band where effective mass is positive and GS exist only for attractive interactions $\sigma = -1$. The small-amplitude GS near the first band-gap edges B, C, in Fig.1 are shown by the corresponding profiles ψ_B and ψ_C depicted in the figure.

As remarked before, the sign of the effective mass determines the type of the interaction of the GS has with the defect potential and for negative GS effective mass (repulsive interatomic interactions) the defect will be seen as a defect trapping potential (supporting therefore bound states) if the defect strength η is positive rather than negative (as seen for the case of a positive effective mass). Except for this, results go in parallel with those of the previous section and have been collected in Figs.5, 7 for the case of an initial GS close the top edge of the first band (negative effective mass). In particular, from the bottom panel of Fig. 5 and Fig. 7 we clearly see that for a fixed defect width the region of the resonant transmission (corresponding to red color) becomes wider as the incoming GS velocity is increased, while the full reflected regions are achieved mainly for small velocities, as one could have expected. We remark that also in this case the number of resonant transmission reflection and trapping regions are found to correlate with the number of impurity modes present in the defect potential for the given range of the defect strength (first four modes corresponding to the maxima of the trapping coefficient C in Fig.5 are depicted in Fig.6, 9).

IV. IMPURITY MODE ANALYSIS AND GS SCATTERING BY OL DEFECTS

As remarked before, the presence of a repulsive (attractive) OL defect in the GPE affects the existing GS states for $\eta = 0$ and introduces additional localized states inside the gap in presence of repulsive (attractive) nonlinearities.

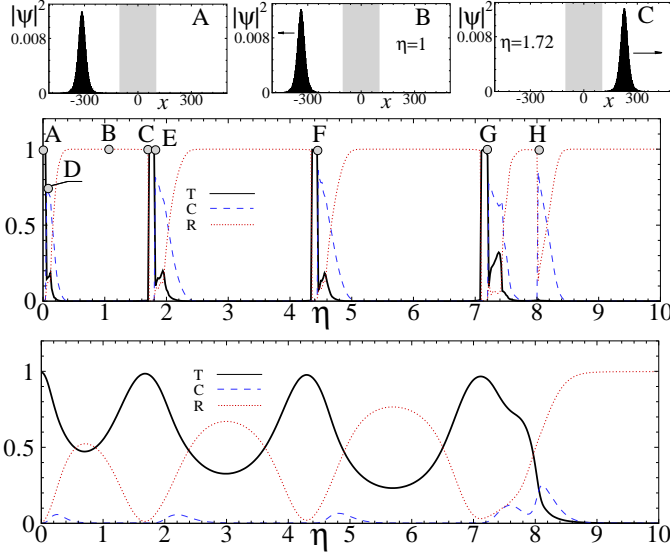


FIG. 5: Dependence of the transmission, reflection and trapping coefficients on the defect amplitude η for $\Delta = 5$ and for two different incoming velocities of the GS ($E_s = 0.475$): $v = 0.02$ (middle panel) and $v = 0.1$ (bottom panel). Top panels A-C show the initial, reflected and transmitted GS profiles, respectively.

Numerical calculations show that the band structure is only slightly affected by an OL impurity, the main effect being the introduction of bound states spatially localized at the impurity sites and with chemical potentials inside the band-gap. Note that repulsive (attractive) OL defects in the presence of an attractive (repulsive) nonlinearity cannot introduce additional bound states because the corresponding impurity potentials correspond to barriers rather than potential wells, due to the positive (negative) effective mass. Recalling that the opposite signs of nonlinearity and effective mass is a necessary condition for the GS existence, one has that the effective impurity potential acts as a trapping potential when η and σ have equal signs. Away from the OL impurity localized states are practically the same as for $\eta = 0$ case. At the defect site, however, GSs levels get slightly shifted by the impurity potential and additional impurity modes enter the gap. A GS moving through the impurity will have, in general, a mismatch in energy and in number of atoms with the impurity modes, this giving a partial reflection/transmission of the incoming matter wave.

A total transparency of the OL defect is expected for incoming GS energies and number of atoms exactly matching those of an impurity modes inside the defect potential (notice that the energy of impurity modes depend on η and on the number of atoms). By increasing the strength of the impurity, the depth of the defect potential increases and more impurity modes enter the gap. As $|\eta|$ is increased, the energies of these modes enter the gap from the top (bottom) of a band for impurity strength and the nonlinearity both positive (negative).

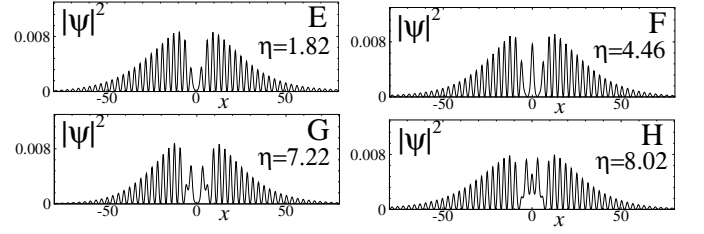


FIG. 6: First four defect modes (panels E-H) in correspondence of maxima of the $C(\eta)$ curve in Fig. 5. Parameters are the same as in Fig. 5.

This implies that the transparency (complete transmission) of the impurity occurs in correspondence of each impurity mode entering the gap and matching the energy of the incoming GS given by

$$E \approx E_s^{(0)} + \frac{1}{2} M_{eff} v_B^2, \quad (6)$$

where the first term $E_s^{(0)}$ represents the energy of the stationary GS state at $k = k_0$ (eg. with $v_B(k_0) = 0$), while the second one is the contribution due to the kinetic energy (here $v_B(k) = dE_\alpha(k)/dk$ is the Bloch velocity and $M_{eff} = (d^2 E_\alpha / dk^2)^{-1}|_{k=k_0}$ the effective mass). For small velocities the energy (6) practically coincides with $E_s^{(0)}$ but in general the kinetic term should be accounted in the matching in energy with the impurity levels (see below). Notice that Eq. (6) is only valid near stationary points k_0 (bottoms or tops of a band) where $v_B(k) \approx (k - k_0)/M_{eff}$ and E can be written as

$$E \approx E_s^{(0)} + \frac{(k - k_0)^2}{2M_{eff}}. \quad (7)$$

In the range of initial velocities $v_B = [0, 0.2]$ we have considered, the energy curves $E_1(k)$ in vicinity of $k_0 = 0$ and $k_0 = 1$ are very well approximated by Eq. (7) with $E_1(0) = -0.12177$, $E_1(1) = 0.47065$, and $M_{eff} \approx 0.565$ and $M_{eff} \approx -0.167$ for bottom and top edges of the band, respectively. By knowing v_B (e.g. k) and M_{eff} one can compute the energy shift due to the nonzero velocity to be accounted in the matching between the GS and the impurity levels (see lower panels of Figs. 8, 9). Notice that the kinetic energy has the sign of the effective mass so that E is pushed forward the corresponding band edge for finite v_B , meaning that inside the impurity potential the GS matching condition with an impurity mode can be achieved for a lower values of $|\eta|$. From this we expect the resonance transmission peaks to be shifted away from the $v = 0$ resonance toward lower values of $|\eta|$ as v_B is increased.

To confirm these prediction with GPE calculations we have solved the stationary problem

$$u_{xx} + [E - V_{ol}(x) - V_d(x)]u - \sigma u^3 = 0 \quad (8)$$

searching for bound states $u(x)$ localized at the OL defect using both shooting method and self-consistent calculations. Using these approaches we found that the values

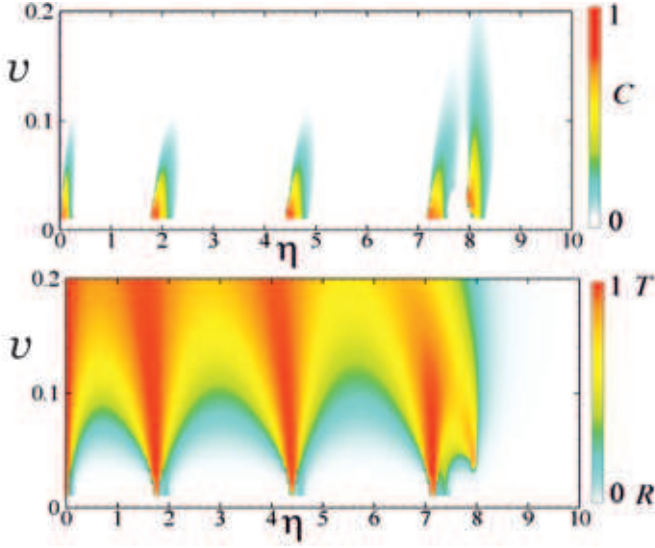


FIG. 7: Dependence of $C(\eta, v)$ (top panel) and $T(\eta, v)$, $R(\eta, v)$ (bottom panel) on η . Parameters are fixed as: $E_s = 0.475$, $\Delta = 5$, $V_0 = -1$, $\sigma = 1$.

of η for which the Gaussian defect becomes transparent to the GS dynamics, correspond to the values for which a localized mode inside the defect potential has energy and number of atoms matching the corresponding quantities of the incoming GS. Since the discussion is very similar (a part implications due to signs of the effective masses) for GS of the semi-infinite and for the ones inside finite-gaps, we refer to the case of an initial GS inside the semi-infinite gap, with a positive effective mass with chemical potential close to the bottom of the first band. In the top panel of Fig.8 we have shown the dependence of the number of atoms N in a defect mode of a given symmetry on η , for an energy $E = E_s = -0.125$ corresponding to a GS with zero incoming velocity (point A of Figs. 1, 3). The horizontal dotted line refers to the numbers of atoms in the initial GS. In the bottom panel of Fig. 8 we show the energy mismatch $|E - E_s|$ between the energy of a defect modes E and the one of an incoming GS given by Eq. 7 for different incoming velocities. Notice that the intersection points A, D, E, F, G of the dotted line $N = N_A$ with the curves $N(\eta)$ are in coincidence with the zeros of the function $|E - E_s|$ displayed in the bottom panel for $v \approx 0$ and correspond to the maxima of the transmission coefficient $T(\eta)$ in Fig.3 (see curves $v \approx 0$ in the middle panel). Fig. 8 (see also 9 for repulsive case) also explains the decay of the reflection coefficient and the rising of the trapping coefficient coinciding up to the maxima observed (just before the resonance) for increasing values of $|\eta|$ away from the resonance points A, D, E, F, G. To the right of these points in Fig.8, the number of particles in the defect mode is higher then the number of particles in the incoming soliton $N(\eta) > N_A$. In this case the GS cannot "use" a defect mode to pass the OL impurity and will be fully reflected. On the left of the resonance points, the number of atoms in the GS is higher than the one in

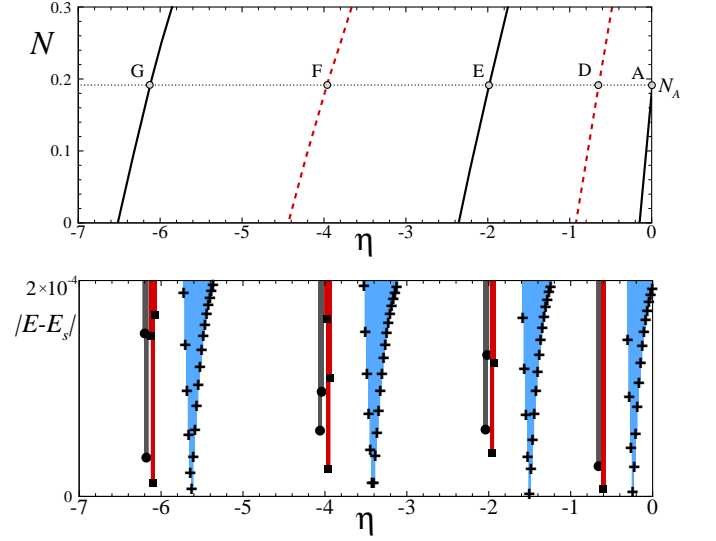


FIG. 8: Top panel. Number of atoms in defect modes vs the amplitude of the defect η . The (black,solid)/(red,dashed) lines correspond to the even/odd symmetry of the defect modes. Other parameters are $E_s = -0.125$, $\Delta = 5$, $V_0 = -1$, $\sigma = -1$. Bottom panel. Mismatch between defect and GS energies, $|E - E_s|$, vs η for different incoming velocities: $v \approx 0$ (gray, \bullet), $v = 0.05$ (red, \blacksquare) and $v = 0.1$ (blue, $+$).

the defect mode so that the GS can be captured by the OL impurity by releasing the excess number of atoms into the reflection and transmission channels. It is clear that the peak of the capture coefficient occurs just before the resonant transmission (e.g. for $0 < N_A - N(\eta) \ll 1$) of the GS through the defect (achieved when the condition $N(\eta) = N_A$ is exactly fulfilled). Notice from Fig.4 that at the resonant transmission, the profiles of the stationary impurity modes obtained by solving Eq.(8) exactly coincide with the solution of the GPE during the passage trough the defect. In Fig.10 we have also depicted, similarly to Fig.2, the level curves $N = N_A$ as a function of the amplitude η and the width Δ of the defect. From the bottom panel of Fig. 8 it is also clear that for $v \neq 0$ the resonances shift in the direction of lower values of $|\eta|$ (as expected from our analysis). This well correlates with the GPE calculations reported in the bottom panel of Fig.3. Similar results are obtained for a GS near the bottom of the first band gap (point B in Fig. 1) for the case of repulsive interactions. This is shown in Fig.9. from which we see that the shift of the resonance due to the finite Bloch incoming velocity is always in the direction of lower values of η and are in good agreement with the GPE numerical results reported in the bottom panel of Fig. 5. In particular, for the velocity $v_B = 0.1$ and the resonance near $\eta = 4$ we obtain from Fig. 9 that the resonance peak is at $\eta \approx 4.45$ while from the GPE result in Fig. 5 we obtain the value $\eta \approx 4.3$. It is also worth to note from the bottom panels of Figs. 8, 9, that for a fixed energy mismatch the widths of the curves increase as the incoming velocity is increased, a fact which correlates

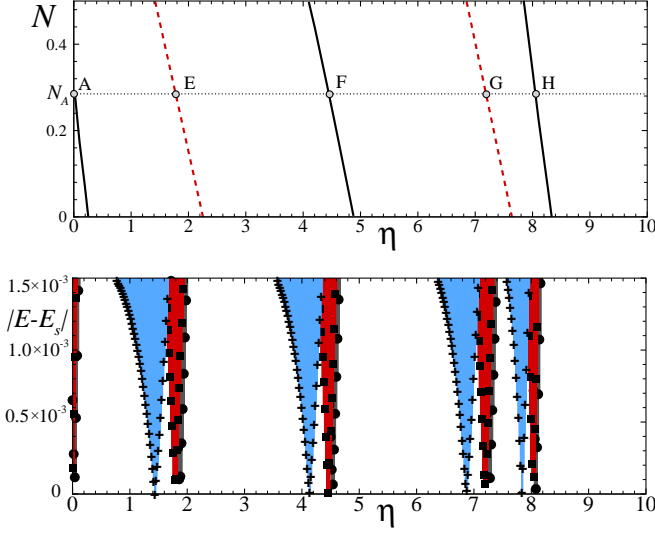


FIG. 9: The same as in Fig.8 but for $E_s = 0.475$ and $\sigma = 1$. The incoming soliton velocities are $v \approx 0$ (gray, \bullet), $v = 0.1$ (red, \blacksquare) and $v = 0.2$ (blue, $+$).

with the broadening of the transmission peaks observed in the GPE calculations (compare bottom panels in Fig. 3 and in Fig 5, respectively).

From this we conclude that the above impurity mode analysis fully confirms the interpretation of the transmission peaks as resonances between incoming GSs and impurity modes.

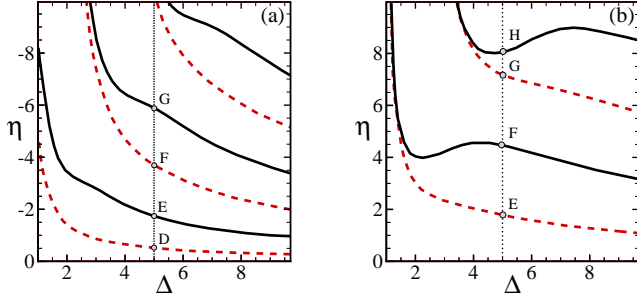


FIG. 10: Level curves $N = N_A$ for even (red, dashed) and odd (black, solid) defect modes $vs (\eta, \Delta)$ for the case of semi-infinite gap (a) and bottom of the first gap (b). Other parameters are fixed as $E_s = -0.125(0.475)$, $V_0 = -1$, $\sigma = -1(1)$.

V. RESONANT TRANSMISSION THROUGH MULTIPLE OL DEFECTS

An interesting question to ask is whether the soliton resonant transmission could survive multiple impurity scatterings. In Fig. 11 we show the transmission, reflection and trapping regions of an attractive GS of the

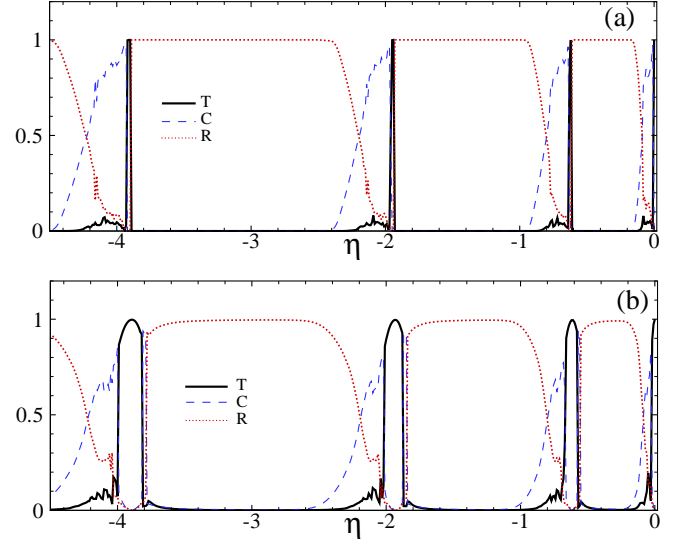


FIG. 11: Transmission, reflection and trapping diagram of GSs with velocities $v = 0.01$ (a) and $v = 0.05$ (b) in presence of two Gaussian defects of the OL placed at positions $x = 0$ and $x = 100\pi$. Other parameters are the same as in Fig.3.

GPE with two identical Gaussian OL impurities, placed at $x = 0$ and $x = 100\pi$, respectively. The TCR curves depend also on the distance between the two impurities and this could be varied so to find optimal values for double resonant transmission to occur. The phenomenon, however, is more sensitive to variations of the incoming GS velocity as one can see by comparing Fig.11 with the case of single impurity in Fig. 3. Notice that while the trans-

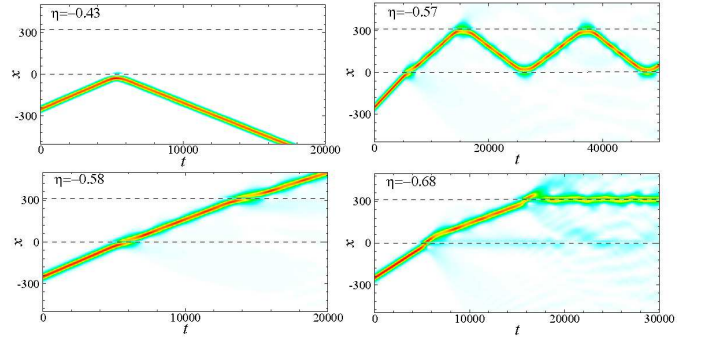


FIG. 12: Contour plot of the GS space-time dynamics for an OL with two equal Gaussian defects of strengths: $\eta = -0.43$ (top left), $\eta = -0.57$ (top right), $\eta = -0.58$ (bottom left), $\eta = -0.68$ (bottom right). The initial velocity of the GSs is $v = 0.05$ and parameters are the same as for Fig. 11 (bottom panel).

mission resonance peaks at small velocities are practically unaffected by the presence of the second impurity, they become more narrow at larger velocities for the resonant scattering on two impurities. The shrinking of the resonances at larger velocities can be understood by the fact that for higher incoming velocities the velocity of the GS

after the first impurity is slightly reduced and the variation introduces a detuning from resonance in the scattering with the second impurity which in turn reduces the double resonance width. From this one can expect that in the presence of more lattice defects the multiple resonance transmission peaks become very narrow and only solitons with very precise initial matching velocities will be able to pass. In general the GS may be able to pass only a finite number of impurities before remaining trapped at one impurity or becoming scattered back and forth between them. This is shown in Fig.12 where contour plots of the GS space-time dynamics in presence of two identical Gaussian defects are reported for different strengths η and for the same parameters as for the bottom panel of Fig.11. In the left top and bottom panels we see the occurrence of total reflection and transmission for a resonant value of η while in the corresponding right panels we show the back and forth dynamics of the soliton between two impurities (top panel) and the trapping by the second impurity (top panel) for a non resonant values of η . Notice the small change of the soliton velocity after the passage through the first defect. To overcome the detuning from resonance induced by the change of velocity one could design the strength of the second impurity so to match the value of the intermediate velocity and still achieving $T \approx 1$. In this way one can realize a double (or multiple) filtering of the soliton motion so that only GSs having very precise initial velocity can overcome the defect series. This possibility is illustrated in Fig. 13

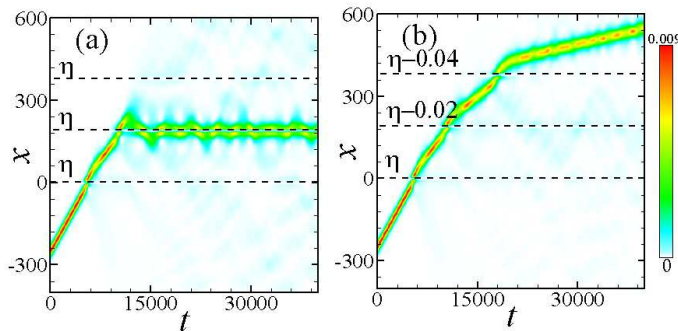


FIG. 13: Panel (a). Contour plot of the GS space-time dynamics in an OL with three equal Gaussian defects at positions $x_1 = 0$, $x_2 = 60\pi$, $x_3 = 120\pi$ of strengths $\eta_1 = \eta_2 = \eta_3 = -0.67$. Panel (b). Case of three different Gaussian defects of strengths $\eta_1 = -0.67$, $\eta_2 = \eta_1 - 0.02$, $\eta_3 = \eta_1 - 0.04$ (b). Other parameters are fixed as in Fig.3.

where the resonant transmission of a GS through a series of three Gaussian defects of the OL, with defect strengths designed so to compensate the detunings introduced by the velocity changes, is shown. Notice from the left panel of Fig. 13 that in the case of equal defects with the initial velocity matching the resonance transmission peak of the first defect, the GS cannot be transmitted through all the three defects but it is stopped at the second defect. The dynamics of the soliton in presence of multiple

defects may be quite complicated and is beyond the aim of this work (an investigation in the parameter space of the possible scenarios for the GS time evolution will be discussed elsewhere).

VI. CONCLUSION

In this paper we have investigated the scattering properties of matter wave gap-solitons with optical lattice defects in the framework of the mean-field Gross-Pitaevskii equation. We have shown that the occurrence of repeated reflection, transmission and trapping regions are in correspondence of the defects strengths for which the number of atoms and energies of additional bound states created by the optical lattice defect, match the ones of the incoming gap-soliton. This has been demonstrated by a study of the stationary defect modes energies (chemical potentials) and number of atoms as a function of the defect strength. A very good agreement between the predicted values of the resonant transmission peaks by means of impurity modes and the ones found by direct time integrations of the Gross-Pitaevskii equation, is found.

The behavior of the reflection and trapping curves have also been explained by impurity mode analysis. These investigations have been performed both for attractive and repulsive interactions and for localized states both in the semi-infinite gap (attractive case) and in the first gap zone (attractive and repulsive cases). The dependence of the resonant transmission on the initial gap-soliton velocity has been also investigated. We have shown that the positions of resonant transmission peaks shift toward lower values $|\eta|$ as the initial gap-soliton velocity is increased, while the widths of resonances shrink to zero at very small gap-soliton velocities. The possibility of multiple resonant transmission through an array of defects was also demonstrated. In particular, we have shown that for an optical lattice with two equally spaced identical Gaussian defects the widths of the full transmission resonances for larger incoming velocities, decreases as the number of defects is increased. The sharpening of the transmission peaks has been explained in terms of the detuning from resonance introduced by the small velocity change after the passage of an optical lattice defect. Finally, the resonant transmission of a gap-soliton through a series of Gaussian defects with unequal strengths designed so to compensate detunings introduced by the velocity changes, was demonstrated. These results give the possibility to construct very precise filters for the matter wave gap-soliton dynamics by means of properly designed arrays of OL defects.

Acknowledgments

V.A.B. acknowledges support from the FCT grant, PTDC/FIS/64647/2006. MS acknowledges the MIUR (PRIN-2008 initiative) for partial financial support.

-
- [1] See review papers O. Morsch and M. Oberthaler, *Rev. Mod. Phys.* **78**, 179 (2006) and references therein; I. Bloch, *J. Phys. B* **38**, S629. (2005); D. Jaksch, and P. Zoller, *Ann. Phys. N.Y.* **315**, 52 (2005); V.A. Brazhnyi and V. V. Konotop, *Mod. Phys. Lett.* **18** 627 (2004).
- [2] M. Greiner, O. Mandel, T. Esslinger, T.W. Hänsch, and I. Bloch, *Nature (London)* **415**, 39 (2002).
- [3] O. Morsch, J. H. Müller, M. Cristiani, D. Ciampini, and E. Arimondo, *Phys. Rev. Lett.* **87**, 140402 (2001); I. Carusotto, L. Pitaevskii, S. Stringari, G. Modugno, and M. Inguscio, *Phys. Rev. Lett.* **95**, 093202 (2005).
- [4] M. Jona-Lasinio, O. Morsch, M. Cristiani, N. Malossi, J. H. Müller, E. Courtade, M. Anderlini, and E. Arimondo, *Phys. Rev. Lett.* **91**, 230406 (2003); S. Wimberger, R. Mannella, O. Morsch, E. Arimondo, A. R. Kolovsky, and A. Buchleitner, *Phys. Rev. A* **72**, 063610 (2005).
- [5] A. Zenesini, H. Lignier, G. Tayebirad, J. Radogostowicz, D. Ciampini, R. Mannella, S. Wimberger, O. Morsch, and E. Arimondo, *Phys. Rev. Lett.* **103**, 090403 (2009).
- [6] B. P. Anderson and M. A. Kasevich, *Science* **282**, 1686 (1998).
- [7] M. Fattori, C. D’Errico, G. Roati, M. Zaccanti, M. Jona-Lasinio, M. Modugno, M. Inguscio, and G. Modugno, *Phys. Rev. Lett.* **100**, 080405 (2008).
- [8] V. V. Konotop and M. Salerno, *Phys. Rev. A* **65**, 021602 (2002).
- [9] B. Eiermann, Th. Anker, M. Albiez, M. Taglieber, P. Treutlein, K. P. Marzlin, and M. K. Oberthaler, *Phys. Rev. Lett.* **92**, 230401 (2004).
- [10] V.A. Brazhnyi, V.V. Konotop, V. Kuzmiak, *Phys. Rev. A* **70**, 043604 (2004).
- [11] M. Salerno, V. V. Konotop, and Yu. V. Bludov, *Phys. Rev. Lett.* **101**, 030405 (2008).
- [12] V. V. Konotop, P. G. Kevrekidis, and M. Salerno, *Phys. Rev. A* **72**, 023611 (2005); V.A. Brazhnyi, V.V. Konotop, V. Kuzmiak, V.S. Shchesnovich, *Phys. Rev. A* **76**, 023608 (2007).
- [13] Yu. V. Bludov, V. V. Konotop, and M. Salerno, *Europhys. Lett.* **87**, 20004 (2009).
- [14] Yu. V. Bludov, V. V. Konotop, and M. Salerno, *J. Phys. B: At. Mol. Opt. Phys.* **42** 105302 (2009).
- [15] Yu. V. Bludov, V. V. Konotop, and M. Salerno, *Phys. Rev. A* **80**, 023623 (2009).
- [16] Yu.V. Bludov, V.V. Konotop, and M. Salerno, *Phys. Rev. A* **81** 053614 (2010).
- [17] B.B. Baizakov, V.V. Konotop, and M. Salerno, *J. Phys. B* **35** 5105 (2002); E.A. Ostrovskaya, Yu.S. Kivshar, *Phys. Rev. Lett.* **90**, 160407 (2003); J. Yang and Z. Musslimani, *Opt. Lett.* **23**, 2094 (2003); B.B. Baizakov, B.A. Malomed, and M. Salerno, *Europhys. Lett.* **63**, 642 (2003).
- [18] A.A. Sukhorukov, Y.S. Kivshar, O. Bang, J.J. Rasmussen, and P.L. Christiansen, *Phys. Rev. E* **63**, 036601 (2001).
- [19] K.T. Stoychev, M.T. Primatarowa, and R.S. Kamburova, *Phys. Rev. E* **70**, 066622 (2004).
- [20] T. Ernst and J. Brand, *Phys. Rev. A* **81**, 033614 (2010).
- [21] T. Iizuka and M. Wadati, *J. Phys. Sot. Jpn.* **61**, 4344 (1992).
- [22] T. Iizuka, H. Amie, T. Hasegawa, C. Matsuoka, *Phys. Lett. A* **220**, 97 (1996).
- [23] M.T. Primatarowa, K.T. Stoychev, and R.S. Kamburova, *Phys. Rev. E* **72**, 036608 (2005).
- [24] Luis Morales-Molina and Rodrigo A. Vicencio, *Opt. Lett.* **31**, 966 (2006).
- [25] A. Trombettoni and A. Smerzi, *Phys. Rev. Lett.* **86**, 2353 (2001); F.K. Abdullaev, B.B. Baizakov, S.A. Darmanyan, V.V. Konotop, and M. Salerno, *Phys. Rev. A* **64**, 043606 (2001).
- [26] A. E. Miroschnichenko, S. Flach, and B. Malomed, *Chaos* **13**, 874 (2003).
- [27] V. Ahufinger, A. Mebrahtu, R. Corbalán and A. Sanpera, *New Journal of Physics* **9**, 4 (2007).
- [28] V. M. Pérez-García, H. Michinel and H. Herrero, *Phys. Rev. A* **57**, 3837 (1998).
- [29] G. L. Alfimov, V. V. Konotop and M. Salerno, *Europhys. Lett.* **58**, 7 (2002).
- [30] M. Salerno, *Laser Physics* **15**, 620 (2005).